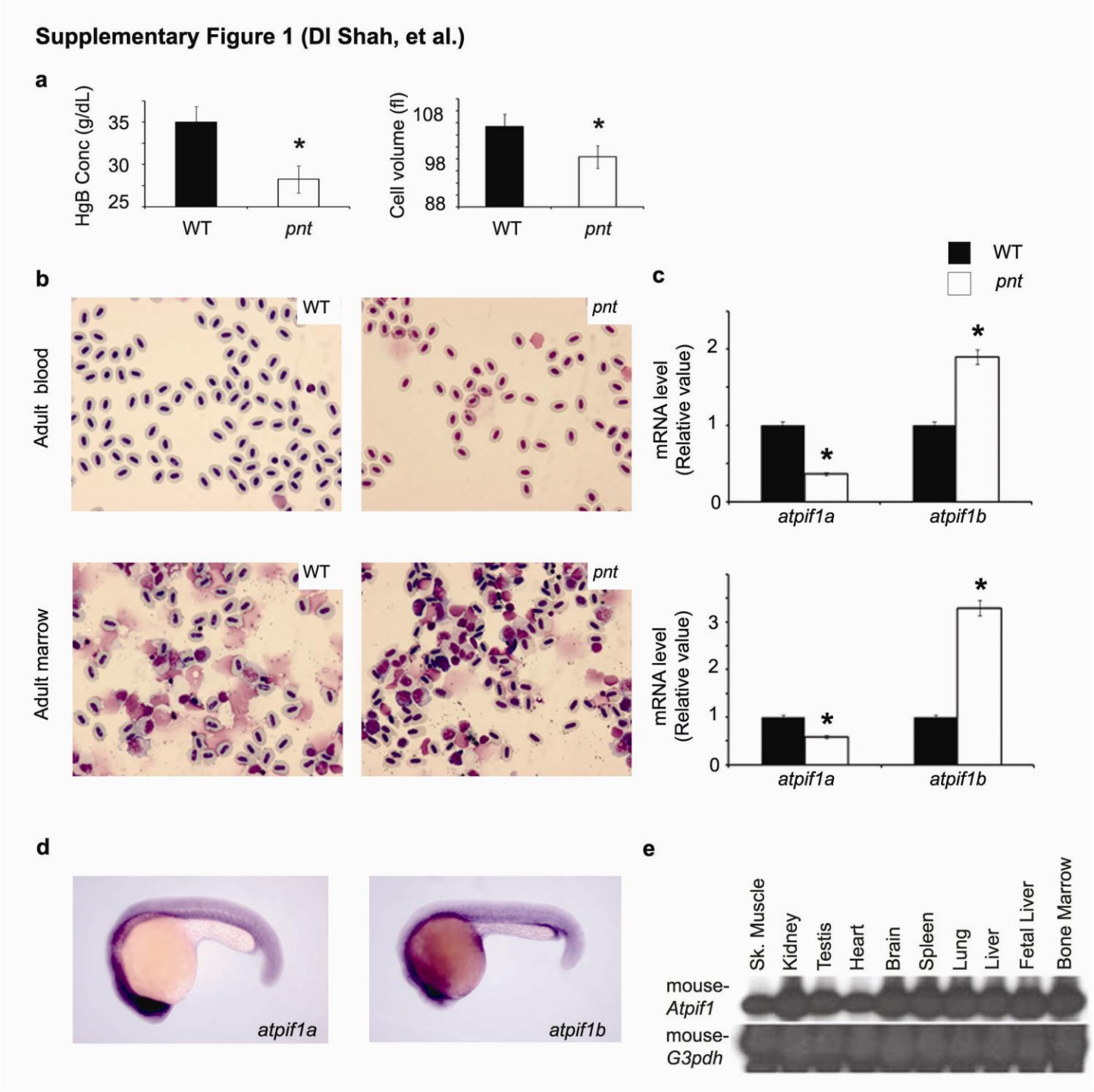

Supplementary Fig. 1 ***Characterization of adult pinotage (pnt) hematopoietic tissues.***
a, *pnt* viable adult blood contains erythrocytes with significantly reduced hemoglobin concentration (HgB, left) and cell volume (right). **b,** Wright-Giemsa staining reveals normal erythroid maturation in adult *pnt* peripheral blood (top) and adult kidney marrows (bottom). **c,** Analysis of *atpif1a* and *atpif1b* mRNA using qRT-PCR. The quantity of *atpif1a* mRNA is reduced in adult *pnt* peripheral blood (top) and adult kidney marrows (bottom) with a compensatory 2 to 3-fold increase in the level of *atpif1b* mRNA. *p<0.05 (t-test, n=3) **d,** Whole-mount *in situ* hybridization shows ubiquitous expression of *atpif1a* (left) and *atpif1b* (right) mRNA in zebrafish WT embryos at 24 hpf. **e,** Semi-quantitative reverse-transcriptase (RT)-PCR analysis demonstrates that Atpif1 is ubiquitously expressed in major mouse organ systems.

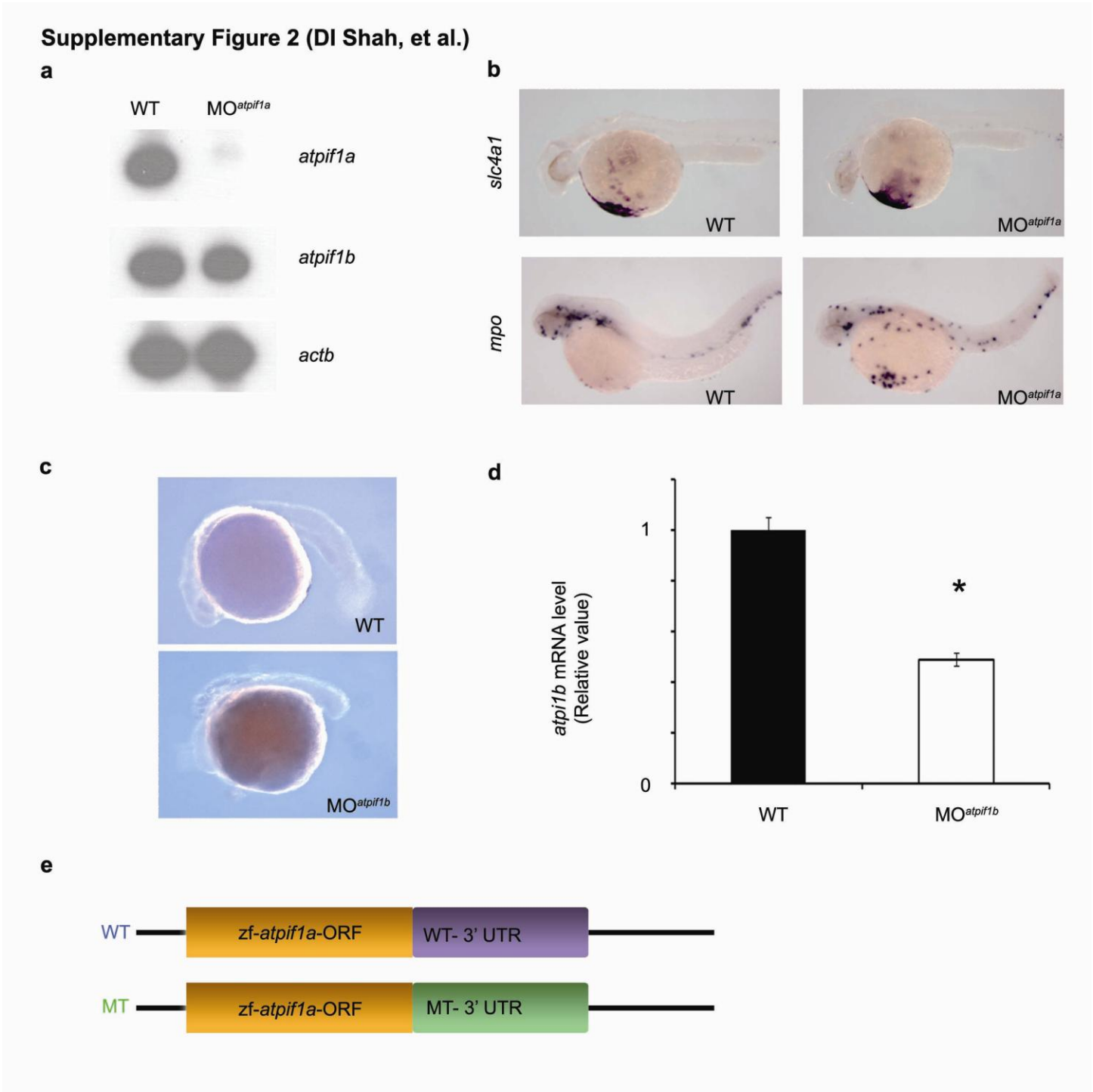

Supplementary Fig. 2 ***Characterization of atpif1 morphants.***

a, The anemic phenotype of the morphant embryos is due to the selective knockdown of *atpif1a.* The *atpif1a* mRNA is degraded in the *atpif1a*-morphant embryos by semi-quantitative reverse-transcriptase (RT)-PCR. The *atpif1a*-morpholino (MO) has no off-target effects on *atpif1b* or *actb* mRNA. **b,** Whole-mount *in situ* hybridization of *slc4a1* (erythroid marker) and *mpo* (myeloid marker) mRNA in wild-type (WT) and *atpif1a*-morphant embryos at 48 hpf. Injection of *atpif1a*-MO has no gross effect on erythroid and myeloid lineage differentiation. **c,** Injection of splice-blocking *atpif1b*-MO severely impairs the normal development of zebrafish embryos at 20 hpf. **d**, qRT-PCR analysis shows that the *atpif1b* mRNA is degraded in *atpif1b*-MO injected embryos, when normalized to *hprt1* mRNA levels. *p<0.05 (t-test, n=3) **e,** Schematics depict the WT and mutant (MT) 3'UTR fused to the zebrafish *atpif1a* open reading frame (ORF).

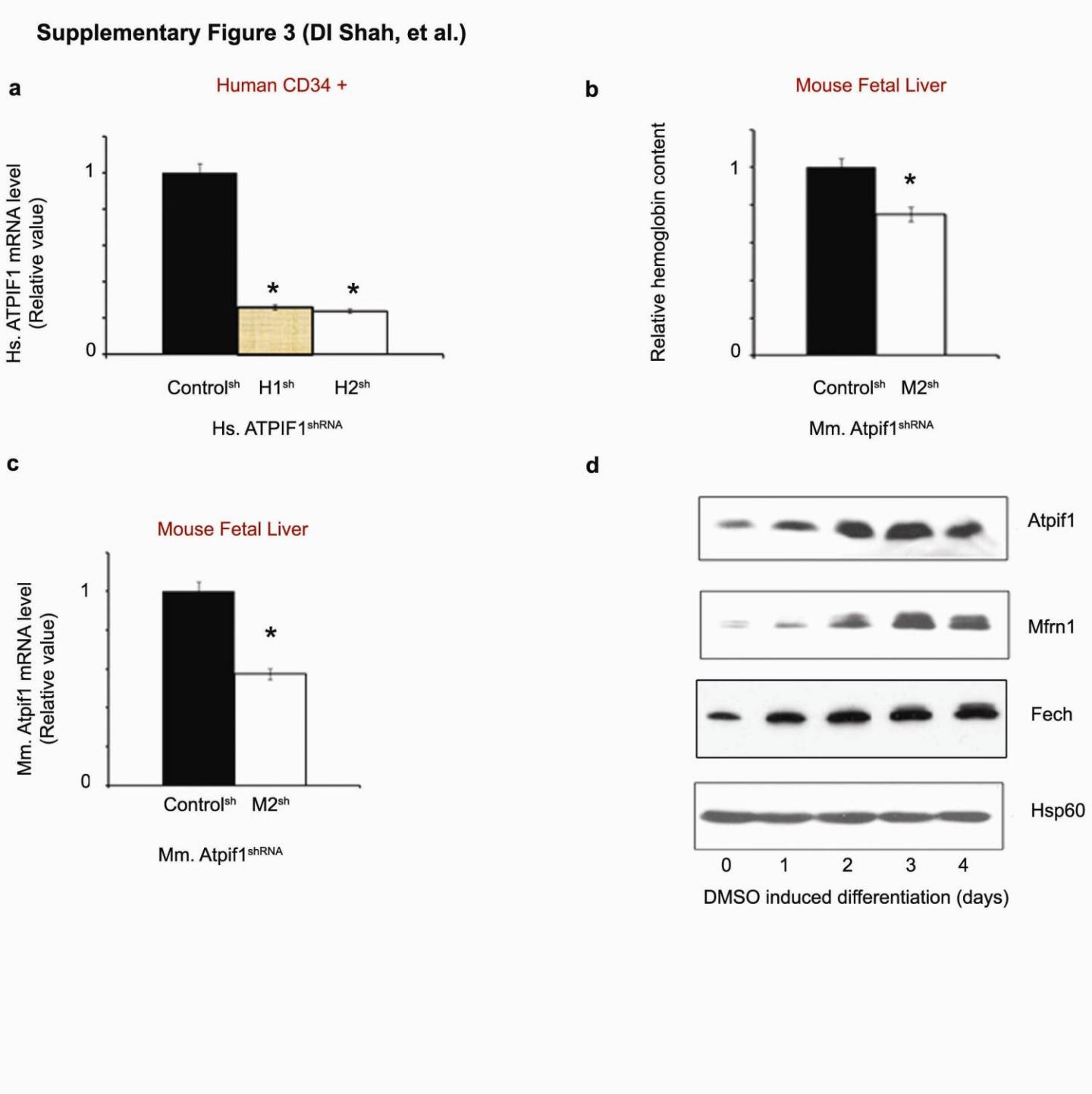

Supplementary Fig. 3 ***Analysis of Atpif1 mRNA levels in Atpif1-shRNA silenced mammalian erythroid cells.***

a, The human-*ATPIF1*-shRNAs ($H1^{sh}$ and $H2^{sh}$) have reduced *ATPIF1* mRNA levels in human primary CD34+ cells. **b,** *Atpif1*-shRNA ($M2^{sh}$) significantly reduces the relative hemoglobin content in mouse primary fetal liver cells. **c,** The mouse-*Atpif1*-shRNA ($M2^{sh}$) has reduced *Atpif1* mRNA in mouse primary fetal liver cells. **d,** The protein expression of Atpif1, Fech, and Mfrn1 is significantly increased in DMSO induced differentiating MEL cells, while mitochondrial Hsp60 remain unchanged. *$p<0.05$ (t-test, n=3)

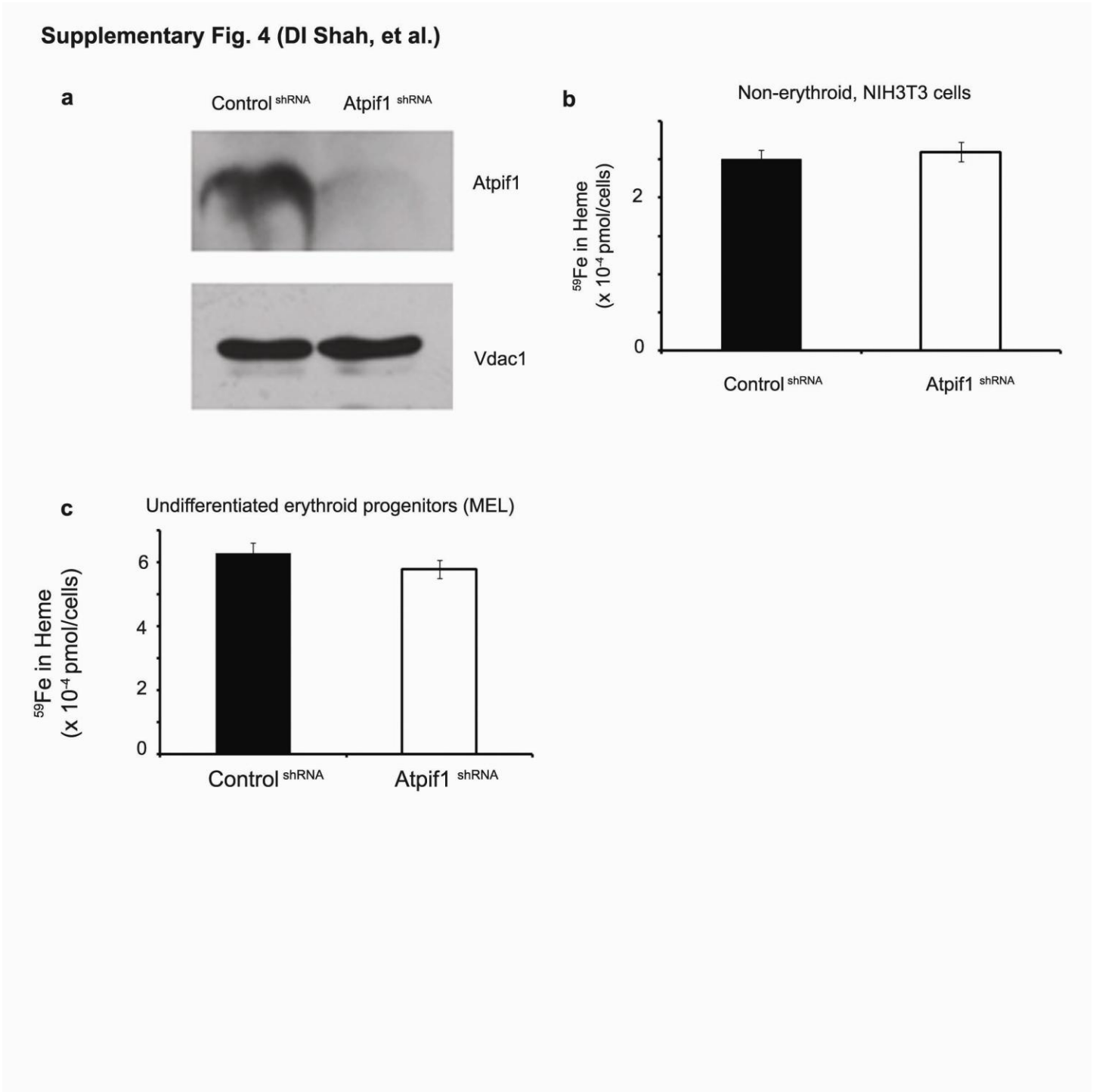

Supplementary Fig. 4 ***Loss of Atpif1 in non-erythroid, NIH 3T3, and undifferentiated MEL cells has no impact on heme synthesis.***

a, Western analysis in Atpif1-shRNA silenced NIH 3T3 cells. Atpif1 protein level is reduced in *Atpif1*-shRNA silenced 3T3 cells. However, mitochondrial structural protein, Vdac1, is not affected. **b,** The levels of ^{59}Fe incorporated in heme are similar in control and *Atpif1*-silenced 3T3- cells **c**, The level of ^{59}Fe incorporated in heme are normal in control and *Atpif1*-silenced undifferentiated MEL- cells.

Supplementary Figure 5 (DI Shah, et al.)

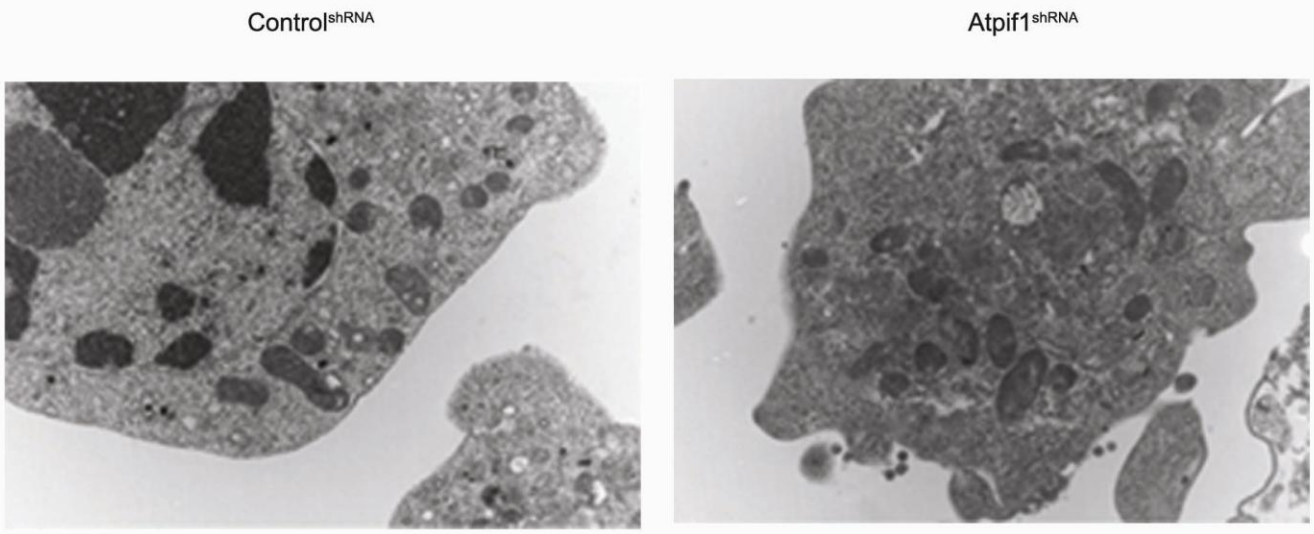

Supplementary Fig. 5 ***Electron microscopic analysis reveals that the structural integrity of mitochondria is intact in the Atpif1-silenced MEL cells.***

The signs of unhealthy mitochondria, such as lipid droplets in cytoplasm or mitochondria, abnormal autophagosome, mitochondrial turnover or abnormal cristae, were absent.

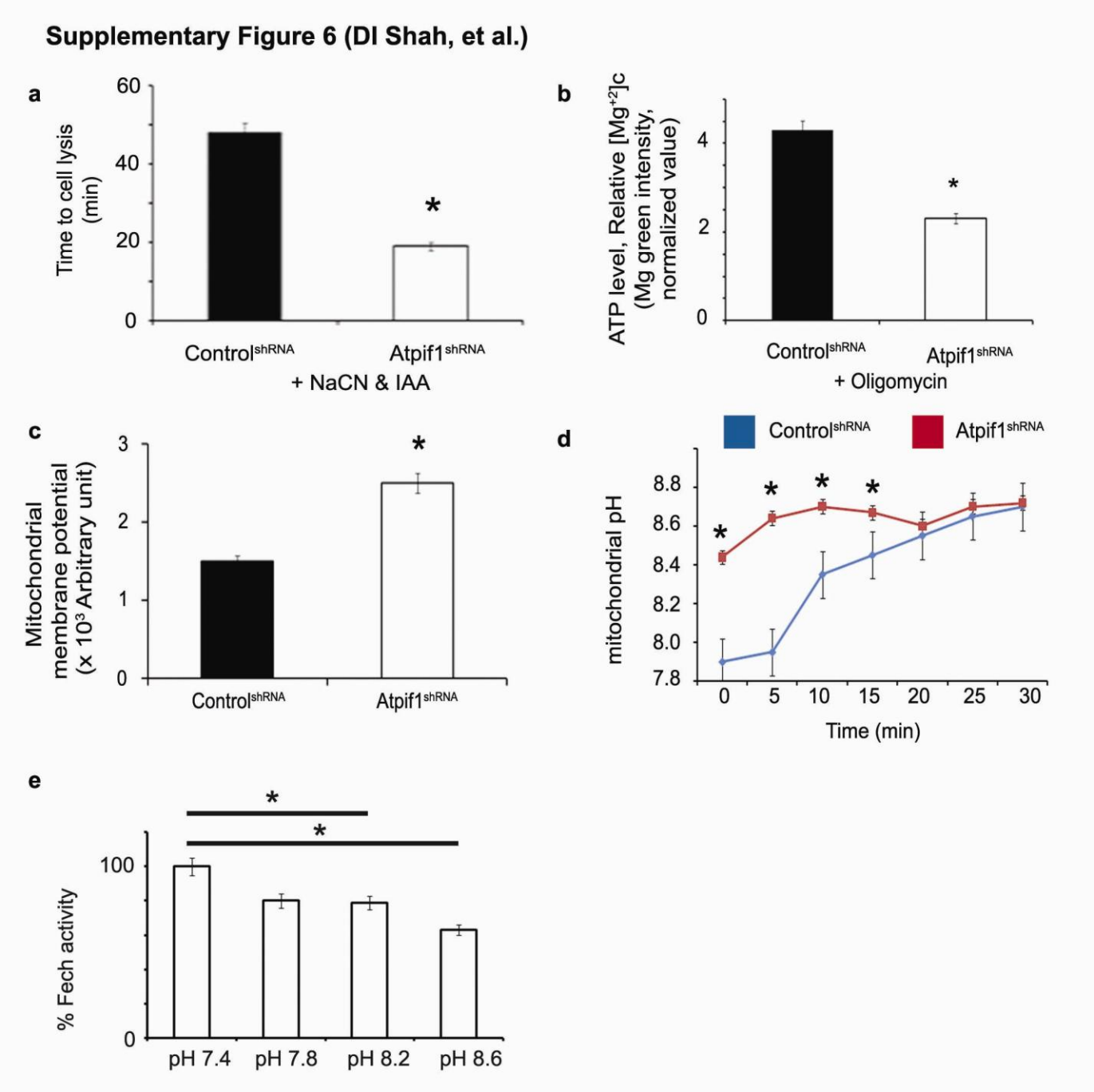

Supplementary Fig. 6 ***Atpif1 regulates mitochondrial physiological parameters.***

a, Cell lysis induced by ATP depletion is faster in the absence of Atpif1. By triggering mitochondrial ATP consumption with NaCN and concomitantly blocking cellular glycolysis with iodoacetic acid (IAA), cellular ATP levels start to fall thus leading to cell death. **b,** The differentiating cells silenced for *Atpif1* deplete ATP faster than the control cells, using the fluorescent Mg indicator Mg Green as a direct function of ATP reduction following oligomycin treatment. **c,** Loss of *Atpif1* elevates mitochondrial membrane potential (ΔΨm). Analysis of mitochondrial ΔΨm using tetramethylrhodamine, methyl ester (TMRM) fluorescent dye following oligomycin treatment used to block the contribution of ATP synthase. **d,** Silencing of *Atpif1* increases mitochondrial matrix pH to 8.5. **e**, The elevated mitochondrial pH reduces vertebrate Fech activity. The pre-incubation of the purified human Fech at elevated pH (7.4, 8.0, 8.5, and 9.0) for 1 hr reduces the Fech activity, verifying that the alkaline pH has negative impact on Fech to make heme. *p<0.05 (t-test, n=3)

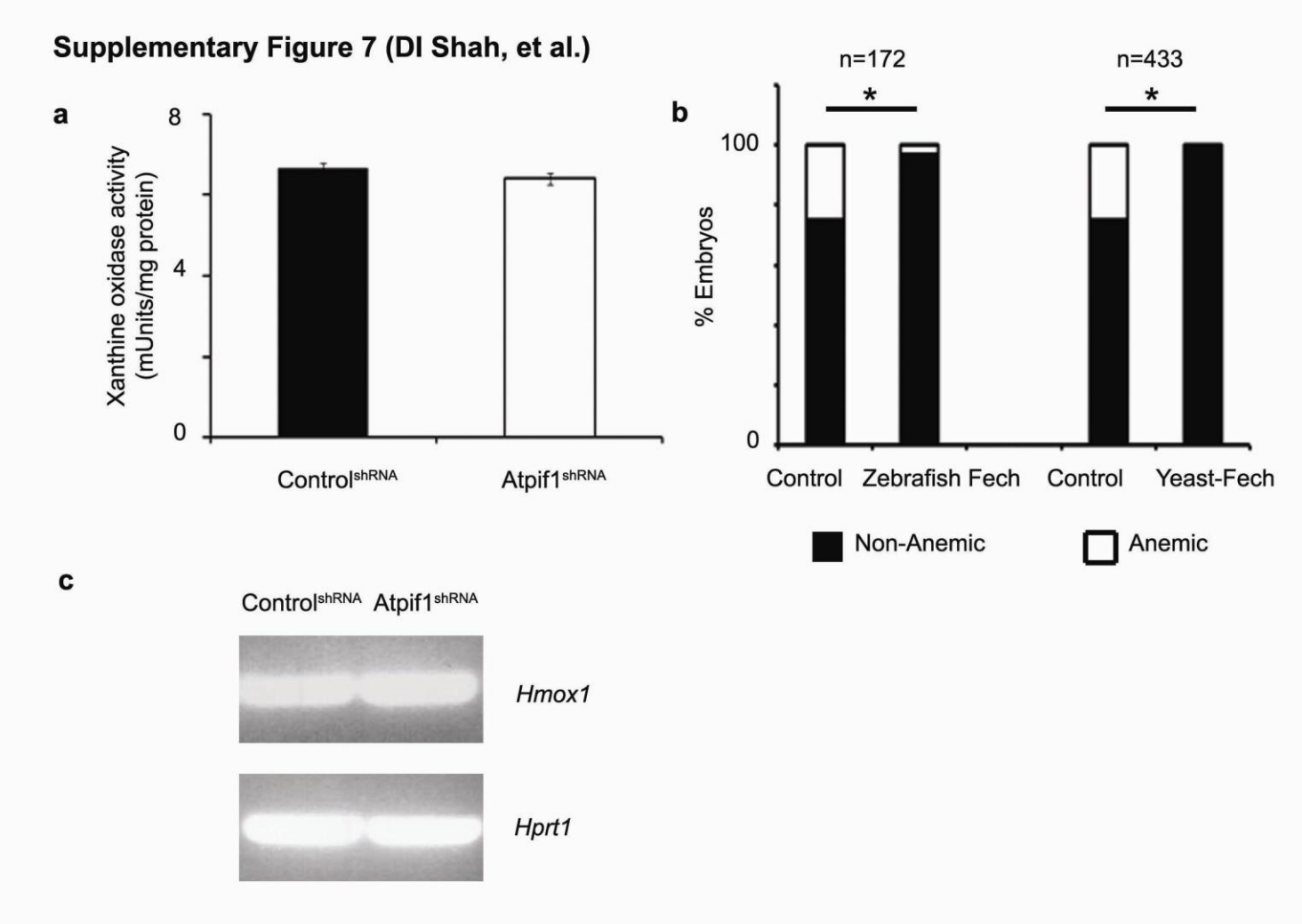

Supplementary Fig. 7 ***Loss of Atpif1 does not impact cytosolic [2Fe-2S] cluster synthesis, and complementation of Fech-deficient zebrafish mutant by either yeast or vertebrate Fech.***

a, Analysis of cytosolic [2Fe-2S] formation as a measure of xanthine oxidase activity. Silencing of *Atpif1* does not affect total cytosolic [2Fe-2S] cluster synthesis as measured by xanthine oxidase activity. **b,** Ectopic expression of zebrafish Fech or yeast Fech complements the anemia in *freixenet* (*frx*^{tu271}) embryos. Functional analysis of yeast Fech and zebrafish Fech constructs, indicating the efficiency of zebrafish Fech and yeast Fech to compensate the loss of zebrafish Fech in *frx* embryos in comparison with un-injected control embryos. *p<0.05 (t-test, n=3) **c,** Semi-quantitative RT-PCR analysis shows that *heme-oxygenase-1* (*Hmox1*) transcript expression is normal in control and *Atpif1*-silenced MEL cells.

SUPPLEMENTARY METHODS

All procedures were approved by the Animal Care and Use Committee of the Boston Children's Hospital.

Zebrafish strains. We recovered *pnt*^{tq209} and *frx*^{tu271} from screens in Tübingen, Germany[1]. *pnt*^{tq209} and *frx*^{tu271}embryos were generated on the AB background, and zebrafish were maintained and staged as described[1, 2].

Isolation, histological staining and phenotypic characterization of blood cells. We obtained *pnt* adult blood and performed Wright-Giemsa staining as described[3]. Cells were collected by centrifugation at 1800 rpm for 10 min and re-suspended in less than 100 µl 0.9x phosphate buffer saline (PBS). Mean corpuscular volume (MCV), and hemoglobin concentration (HgB) were determined using an ADVIA 120 Hematology Analyzer (Siemens Diagnostic Solutions, Tarrytown, NY).

Genetic mapping and positional cloning. We meiotically mapped the *pnt* locus to zebrafish chromosome 19 (Chr. 19) using bulk segregant analyses as described[2, 3]. Bioinformatics analysis annotated the *pnt* locus (z*gc: 162207*) as the mitochondrial *ATPase inhibitory factor 1* (*atpif1a*) (NM_001089521.1). A zebrafish paralog, *ATPase inhibitor factor 1-like protein* (*atpif1b*) (NM_001044859), was identified from the GenBank database and obtained from Open Biosystems (Huntsville, AL).

Mutational analysis. We isolated total RNA from wild-type (WT) and *pnt* embryos at 3–4 days post-fertilization (dpf) and analysed the cDNA as described[2,3]. Primer sequences for amplification and genotyping information are available from the authors on request. The distinct segregation of WT and mutant (MT) genotype showed linkage by single-strand conformational polymorphism (SSCP) and single-strand length polymorphism (SSLP) analysis. The zebrafish *atpif1a* constructs with either WT or polymorphic 3'UTR sequences were transfected into Friend mouse erythroleukemia (MEL) cells, and the stable clones were selected by puromycin selection. The qRT-PCR analysis was performed to assay target mRNA in stable *atpif1a* mRNA levels in cells harboring polymorphic 3'UTR constructs as compared to the WT construct.

In situ hybridization and *o*-dianisidine staining. We carried out zebrafish whole-embryo *in situ* hybridization with *atpif1a, scl4a1* (*band-3*), *β-globin*, and *mpo* digoxigenin labeled probes as described[2, 3]. We stained live embryos with *o*-dianisidine at 2–4 dpf as described[4].

cRNA injections for over-expression in zebrafish. We sub-cloned cDNA clones for zebrafish *atpif1a*, E26A-*atpif1a*, *atpif1b*, *Fech*, and yeast Fech into a pCS2^{+}-CMV vector. We prepared 5' -capped cRNA using the SP6 mMessage mMachine kit (Ambion, Austin, TX). Fertilized eggs from *pnt*^{tq209} heterozygous pairs were injected at the 1-2-cell stage with ~100 pg of cRNA and phenol red dye as a tracer as described[2].

Morpholino knockdown in zebrafish. An antisense morpholino complementary to the splice-donor site of *atpif1a*-exon 2 (5'- TACCCAGCTCACCCAGCTGCACACA-3'), *atpif1a*-translational initiator site (5'-CCTGAGCAGAAGGCGAGCCATGATC-3'), and *atpif1b*-exon 1

(5'-TTCACCTAACTTTATCAGAGAGAGA-3') were synthesized by Gene Tools (Philomath, OR). A standard morpholino provided by Gene Tools was used as a negative control: 5'-CCTCTTACCTCAGTTACAATTTATA-3'. Injected (morpholino doses at 0.5–1mM) and control embryos were either fixed at 24 or 48 hpf for whole-embryo *in situ* hybridization or stained with *o*-dianisidine at 2 dpf.

Antibodies and Drugs. Antisera against mitochondrial Atpif1 (sc-81875), Vdac1 (sc-11433), Fech (sc-49663), and Hsp60 (sc-1722) were purchased from Santa Cruz Biotechnology (Santa Cruz, CA) whereas antisera against AtpB (ab14730) and CoxIV (ab16056) were purchased from Abcam (Cambridge, MA). Antisera against Mfrn-1 were prepared as previously described[2]. 2,4-dinitro-phenol (2,4-DNP), and sodium dithionite (DTN) were purchased from Sigma-Aldrich (St. Louis, MO). Recording medium contained 138 mM NaCl, 5.6 mM KCl, 4.2 mM $NaHCO_3$, 1.2 mM NaH_2PO_4, 1.2 mM $MgCl_2$, 2.6 mM $CaCl_2$, 10 mM glucose, 10 mM HEPES, pH 7.4. Poly-L-lysine solution was from SIGMA-ALDRICH® Co. (Saint Luis, MO). Ø 22 mm borosilicate cover slips were from VWR International Srl (West Chester, PA). 5-(and-6)-carboxy SNARF®-1, acetoxymethyl ester, acetate; Magnesium Green™, AM (cell permeant); Mito Tracker® Green FM; Tetramethylrhodamine, methyl ester, perchlorate (TMRM) were from Invitrogen™ by Life Technologies™ Inc. (Paisley, UK). Carbonyl cyanide 4-(trifluoromethoxy)phenylhydrazone (FCCP); Dimethyl sulfoxide (DMSO); Iodoacetic acid; Nigericin sodium salt; Oligomycin A; Sodium cyanide; were from SIGMA-ALDRICH® Co. (Saint Luis, MO). LSM 510 Confocal Laser Scanning Microscope (inverted configuration on an Axiovert 200 frame) and LSM Image Browser (live-cell imaging analysis software) were from Carl Zeiss MicroImaging GmbH (Jena, Germany).

shRNAs. Targeted sequences of shRNAs (Sigma-Aldrich, St. Louis, MO), against mouse *Atpif1* (M1:CCGGGACCACCATTCGAAGGAGATACTCGAGTATCTCCTTCGAATGGTGGTCTTTTTTG,M2:CCGGCGTCTGCAGAAGCAAATTGAACTCGAGTTCAATTTGCTTCTGCAACGTTTTTTG) and human *ATPIF1* (H1: CCGGCGCCATAAGCAGAAGATCAAACTCGAGTTTGATCTTCTGCTTATGGCGTTTTTTG; H2: CCGGGATATTTCCGAGCACAGAGTACTCGAGTACTCTGTGCTCGGAAATATCTTTTTTG) were used to silence *Atpif1* or *ATPIF1* in corresponding mammalian erythroid tissues.

Mitochondrial physiology parameters. The mitochondrial membrane potential ($\Delta\Psi m$) was analyzed using a tetramethylrhodamine, ethyl ester (TMRE) fluorescent probe following procedures described earlier[5]. The ratios of fluorescent intensities from cells treated in the presence of verapamil and FCCP are measured. Verapamil, the L-type calcium channel blocker, was used to block the release of Ca^{2+} whereas FCCP, a potent reversible inhibitor of mitochondrial oxidative phosphorylation, was used to depolarize mitochondrial membrane potential. We also measured $\Delta\Psi m$ using tetramethylrhodamine, methyl ester (TMRM) fluorescent dye following oligomycin treatment used to block contribution of ATP synthase.

Measurement of mitochondrial matrix pH

Mitochondrial matrix pH was assessed using the cell-permeant pH indicator probe 5-(and-6)-carboxy SNARF®-1, AM acetate. After terminal differentiation, cells were seeded on poly-L-lysine coated cover slips and, following overnight growth at 37 °C, 5% CO_2, co-loaded with 10

μM carboxy SNARF®-1, AM acetate and 200 nM Mito Tracker® Green, FM in recording medium (30 min incubation at 37 °C, 5% CO_2). After 30 min incubation, the dye was removed and cells were incubated in recording medium for 2.5 h to allow the hydrolysis of cytosolic carboxy SNARF®-1, AM acetate and the preferential compartmentalization of the probe into the mitochondria. Cover slips were then prepared for live cell imaging as described above. Cells were imaged using a "Fluar" 40x/1.30 oil immersion objective; to avoid contamination between carboxy SNARF®-1, AM acetate and Mito Tracker® Green, FM emissions, a sequence of three consecutive scans was performed throughout, using a green Helium-Neon laser (543 nm line) for the former and an Argon laser (488 nm line) for the latter. In order to minimize photobleaching and phototoxicity as much as possible -while still maintaining discernable image- laser power was kept as low as possible, such as 0.1-2%. Fluorescence emission of carboxy SNARF®-1, AM acetate at 590 and 680nm was captured in two consecutive scans through the HTF 488/543 dichroic mirror with BP 565/615 band pass filter and LP 650 high pass filter. Mito Tracker® Green, FM, whose staining was used to select only mitochondrial pixels and derive the mitochondrial calibration curve avoiding contaminations from cytosolic signal, through the HTF 488/543 dichroic mirror with BP 510/520 band pass filter.

In situ pH calibration of carboxy SNARF®-1, AM acetate was performed using differentiated control cells[6]; the pH of the solution was set to four different values (6.0, 7.0, 8.0 and 9.0) and the calibration was performed both from low to high pH and vice versa. Averaged SNARF®-1, AM acetate ratios (680/590 nm) were plotted against pH values to build up the calibration curve and measure mitochondrial matrix pH_m of both MEL clones (maintaining the same settings, chosen to minimizing bleaching). Basal pH_m measurements of both clones were performed in recording medium; 2.5 μg/ml Oligomycin was then added to the medium to evaluate the

contribution of ATP synthase to mitochondrial matrix pH, and images were acquired every 5 min to obtain a pH_m time course. Emission intensities were quantified with the LSM Image Browser software.

Measurement of cellular ATP

ATP levels were indirectly measured with the cell-permeant green-fluorescent Mg^{2+} indicator Magnesium Green™, AM. Differentiated MEL cells were seeded on poly-L-lysine coated cover slips and, following overnight growth at 37 °C, 5% CO_2, co-loaded with 5 µM Magnesium Green™, AM and 50 nM TMRM in recording medium; after incubation, cover slips were then prepared for live cell imaging as described above. To avoid contamination between fluorescent dyes emission, two consecutive scans were performed throughout, using an Argon laser (488 nm line) for Magnesium Green™, AM and a green Helium-Neon laser (543 nm line) for TMRM. The fluorescence emission of Magnesium Green™, AM was captured through the HTF 488/543 dichroic mirror with BP 500/550 band pass filter and TMRM through the HFT 488/543 dichroic mirror with BP 535/590 band pass filter. ATP depletion was induced by adding 2.5 µg/ml oligomycin to block the proton flux through the F_1F_0-ATPsynthase, and images were acquired every second to follow the time-course of cytosolic ATP depletion (TMRM staining was used to subtract mitochondrial pixels from the cellular ROIs analyzed). 2 mM iodoacetic acid (IAA) and 1mM sodium cyanide (NaCN) were instead used to block glycolysis and trigger reversion of the F_1F_0-ATPsynthase to promote consumption of ATP by mitochondria[5, 6]. In this case acquisitions were run every second until cell lysis.

Index of heme synthesis in mammalian cells. We stained dimethyl sulfoxide (DMSO) differentiated MEL or erythropoietin (EPO) differentiated hCD34+ cells with *o*-dianisidine and measured number of hemoglobinized cells as previously described[7]. We also measured level of hemoglobin content in mouse primary fetal liver cells using Drabkin's reagent following procedures previously described[8].

Quantification of heme substrates and its biosynthesis. ^{59}Fe saturated transferrin was prepared as described using ^{59}FeCl3 (>5Ci [185GBq]/g, Perkin Elmer, MA)[9]. Metabolic labeling of *Atpif1*-shRNA and non-targeting-shRNA transfected MEL cells (~2 x 10^6) was done as described[9]. ^{59}Fe incorporated in mitochondria or complexed as heme was quantified using a gamma counter[9]. The cells were homogenized and crude mitochondria were isolated as described[9]. The 25 μg of mitochondria was re-suspended in the assay buffer at variable pH, and incubated with ascorbic acid, NADH, $^{59}FeCl_3$, and deuteroporphyrin IX for 15 min at 37 ^{0}C. The reaction was stopped by adding excess of $FeCl_3$, and ^{59}Fe incorporated heme was extracted and measured as described[9]. We also performed the spectro-photometric analysis of PPIX levels in MEL cells grown with external ALA as previously described[10]. In addition, we examined xanthine oxidase and aconitase activities as a measure of cytosolic and mitochondrial [2Fe-2S] cluster levels, respectively, following the procedures previously described[11]. The catalytic efficiency of Fech was assayed on crude cell extracts of MEL cells grown with ALA supplement. The Fech activity was measured by the real time direct spectroscopic technique previously described[12, 13]. Divalent nickel, rather than ferrous iron, was employed to avoid oxidation issues that may arise with ferrous iron. Formation of metallated porphyrin product was monitored at 550nm. For some assays (Fig. 4a) mitochondria were isolated by differential

centrifugation from disrupted MEL cells and then suspended by sonication in buffer containing 1.0% (wt/vol) sodium cholate. For assays that examined the effect of the reducing agent, sodium dithionite on Fech activity, purified human-Fech or yeast-Fech were used at a final assay concentration of 1 μM[12, 13]. All assays contained 0.1% (wt/vol) Triton X-100. Sodium dithionite and substrates were freshly prepared and assays were run at 25 ^{0}C. All reagents were added to the assay cuvette, mixed and the reaction was then initiated by the rapid addition with mixing of enzyme preparation. All assays were performed in triplicate.

Statistical analyses. Statistical analyses were performed by paired or un-paired t-test. Significance was set at $p<0.05$.

SUPPLEMENTARY DISCUSSION

1) The specificity of the splice-blocking *atpif1a*-MO was further verified by semi-quantitative RT-PCR assay, indicating that the MO was specific for *atpif1a* and had no off-target effects, including *atpif1b* (Supplementary Fig. 2a). In addition, whole mount *in situ* hybridization showed normal expression of *band3* (*slc4a1*, marker for erythroid lineage) and myeloperoxidase (*mpo*, marker for myeloid lineage) in *atpif1a* morphant embryos (Supplementary Fig. 2b), indicating that erythroid and myeloid specification were unaffected by the *atpif1a*-MO. Therefore, *atpif1a* likely plays an important role in erythroid differentiation rather than specification. These findings provide strong evidence that *atpif1a* is responsible for the observed anemia in the *pnt* embryos. In contrast, the injection of a MO targeting *atpif1b* results in general developmental abnormalities and ultimately a lethal phenotype (Supplementary Fig. 2c). The *atpif1b* mRNA expression level was also reduced in *atpif1b*-morphant embryos (Supplementary Fig. 2d). Together, *atpif1b* seems to be essential for embryonic development, while the role of *atpif1a* is highly specific to erythroid cells.
2) Analogous results were obtained using GFP fused with WT and polymorphic 3'UTR sequences (data not shown).
3) Interestingly, we found that the Fech activity in control cells was not reduced at the elevated pH 8.5. We hypothesized that this may be due to the availability of more cellular ATP in control cells to preserve mitochondrial homeostasis, in part by maintaining the mitochondrial pH. To test this hypothesis, we treated control and *Atpif1*-silenced MEL cells with oligomycin to inhibit ATP synthesis[14], and measured their cellular ATP levels and basal mitochondrial matrix pH. Consistent with previous

reports[15, 16], we found faster depletion of ATP levels in oligomycin treated *Atpif1*-silenced MEL cells than the control cells (Supplementary Figs. 6a-6b). This indicates that (1) oxidative phosphorylation provides most of the ATP required in differentiating MEL cells, thus supporting that the Atpif1-mediated changes in respiration are linked to the production of ATP by the ATP synthase; (2) *Atpif1*-silenced MEL cells are more dependent on mitochondrial ATP than control cells, and (3) the control cells have more total cellular ATP to utilize than *Atpif1*-silenced MEL cells. We further found that the oligomycin treatment of control and *Atpif1*-silenced MEL cells elevated the basal mitochondrial pH of only control cells from pH 7.4 to pH 8.6; however, the pH of *Atpif1*-silenced MEL cells remained stable at pH 8.6 (Fig. 4b). This suggested that the additional cellular ATP available to control cells allowed them to preserve mitochondria milieu. The control cells did not show a difference in heme production at pH 8.0 or pH 8.5 (Fig. 4c) because they have normal ATP levels (Supplementary Figs. 6a-6b). When we treated the control cells with oligomycin, we found that Fech activity in oligomycin treated cells was significantly reduced compared to control cells without oligomycin treatment (Fig. 4c). This suggested that the Fech activity is, in part, dependent upon basal ATP levels. Together, ATP levels influence mitochondrial bioenergetics, and thus the mitochondrial milieu, such that the presence of ATP preserves the mitochondrial Fech activity in control cells at a greater extent, whereas the reduction of ATP reduces Fech activity in *Atpif1*-silenced MEL cells.

4) Fech is a homodimer bound to the inner mitochondrial membrane with its active site facing into the membrane[17]. High-resolution crystal structures of human Fech have revealed that the [2Fe-2S] cluster is not within the active site pocket but is located near

the dimer interface in a solvent-filled channel[17]. The structure of Fech further reveals that the two independent active sites of the homodimer may be linked through these solvent-filled channels (data not shown).

REFERENCES FOR SUPPLEMENTARY METHODS & DISCUSSION

1. Ransom, D. G. et al. Characterization of zebrafish mutants with defects in embryonic hematopoiesis. *Development* **123**, 311-9 (1996).
2. Shaw, G. C. et al. Mitoferrin is essential for erythroid iron assimilation. *Nature* **440**, 96-100 (2006).
3. Donovan, A. et al. Positional cloning of zebrafish ferroportin1 identifies a conserved vertebrate iron exporter. *Nature* **403**, 776-81 (2000).
4. Iuchi, I. & Yamamoto, M. Erythropoiesis in the developing rainbow trout, Salmo gairdneri irideus: histochemical and immunochemical detection of erythropoietic organs. *J. Exp. Zool.* **226**, 409-17 (1983).
5. Campanella, M. et al. IF1, the endogenous regulator of the F(1)F(o)-ATPsynthase, defines mitochondrial volume fraction in HeLa cells by regulating autophagy. *Biochim. Biophys. Acta.* **1787**, 393-401 (2009).
6. Campanella, M. et al. Regulation of mitochondrial structure and function by the F1Fo-ATPase inhibitor protein, IF1. *Cell Metab.* **8**, 13-25 (2008).
7. Narla, A. et al. Dexamethasone and lenalidomide have distinct functional effects on erythropoiesis. *Blood* **118**, 2296-304 (2011).
8. Hattangadi, S. M., Burke, K. A. & Lodish, H. F. Homeodomain-interacting protein kinase 2 plays an important role in normal terminal erythroid differentiation. *Blood* **115**, 4853-61 (2010).
9. Chen, W. et al. Abcb10 physically interacts with mitoferrin-1 (Slc25a37) to enhance its stability and function in the erythroid mitochondria. *Proc. Natl. Acad. Sci. U S A* **106**, 16263-8 (2009).

10. Troadec, M. B. et al. Targeted deletion of the mouse Mitoferrin1 gene: from anemia to protoporphyria. *Blood* **117**, 5494-502 (2011).
11. Li, L. & Kaplan, J. A mitochondrial-vacuolar signaling pathway in yeast that affects iron and copper metabolism. *J. Biol. Chem.* **279**, 33653-61 (2004).
12. Najahi-Missaoui, W. & Dailey, H. A. Production and characterization of erythropoietic protoporphyric heterodimeric ferrochelatases. *Blood* **106**, 1098-104 (2005).
13. Burden, A.E. et al. Human ferrochelatase: crystallization, characterization of the [2Fe-2S] cluster and determination that the enzyme is a homodimer. *Biochim. Biophys. Acta* **1435**, 191-7 (1999).
14. Grover, G. J., Marone, P. A., Koetzner, L. & Seto-Young, D. Energetic signalling in the control of mitochondrial F_1F_0-ATP synthase activity in health and disease. *Int. J. Biochem. Cell Biol.* **40**, 2698-701 (2008).
15. Campanella, M., Parker, N., Tan, C. H., Hall, A. M. & Duchen, M. R. IF(1): setting the pace of the F(1)F(o)-ATP synthase. *Trends Biochem. Sci.* 34, 343-50 (2009).
16. Formentini, L., Sanchez-Arago, M., Sanchez-Cenizo, L. & Cuezva, J. M. The Mitochondrial ATPase Inhibitory Factor 1 Triggers a ROS-Mediated Retrograde Prosurvival and Proliferative Response. *Mol. Cell* **45**, 731-42 (2012).
17. Lanzilotta, W.N. & Dailey H.A. Human ferrochelatase in *Handbook of Metalloproteins*, (ed. Messerschmidt, A.) **4&5**: 138-146 (John Wiley & Sons, Ltd, Chichester, UK, 2011).